P H Y S I C A L R E V I E W L E T T E R S

Benchmarking Quantum Control Methods on a 12-Qubit System

C. Negrevergne,[1] T. S. Mahesh,[2] C. A. Ryan,[1] M. Ditty,[1] F. Cyr-Racine,[1] W. Power,[1] N. Boulant,[2]
T. Havel,[2] D. G. Cory,[2] and R. Laflamme[1,3]

[1]*Institute for Quantum Computing, University of Waterloo, Waterloo, ON, N2L 3G1, Canada*
[2]*Department of Nuclear Engineering, MIT, Cambridge, Massachusetts 02139, USA*
[3]*Perimeter Institute for Theoretical Physics, Waterloo, ON, N2J 2W9, Canada*
(Received 17 December 2005; published 1 May 2006)

In this Letter, we present an experimental benchmark of operational control methods in quantum information processors extended up to 12 qubits. We implement universal control of this large Hilbert space using two complementary approaches and discuss their accuracy and scalability. Despite decoherence, we were able to reach a 12-coherence state (or a 12-qubit pseudopure cat state) and decode it into an 11 qubit plus one qutrit pseudopure state using liquid state nuclear magnetic resonance quantum information processors.

Quantum mechanics promises information processors that are more efficient than any known classical devices. However, to bring this potential to reality, we must learn how to control large quantum systems in a scalable fashion. Scalability has at least two components: the complexity of the methods used to obtain coherent control must grow only polynomially with the number of qubits involved, and the errors occurring during the implementation of the control sequence must be small enough to be correctable. These errors can be split in two classes: first, the operational errors due to imperfections in the control procedure and, second, intrinsic errors due to decoherence and relaxation processes. Benchmarking small quantum information processor (QIP) prototypes [1–4] is therefore crucial to characterizing the errors in a physical system and developing general quantum control methods. In a physical system well suited for implementing a QIP, once we have reached an optimal operational control, we will need to take care of intrinsic errors using quantum error correction procedures [5].

Because they have the ability to run nontrivial quantum algorithms, liquid state nuclear magnetic resonance (NMR) based QIPs [6,7] can be used as benchmark systems [1,8,9]. In the present work, we are interested in optimizing operational control strategies in terms of accuracy and the amount of required classical resources. To do so, we have chosen to extend the benchmarking algorithm previously used on a 7-qubit liquid state NMR register [1] to 11 qubits plus one qutrit. This algorithm consists of preparing mixtures of generalized Greenberger-Horne-Zeilinger (GHZ) states of the form: $\rho_{\text{GHZ}} = \mathbf{I}^{\otimes n} + \mathbf{X}^{\otimes n}$ (**I** is the identity matrix, **X** is the $\boldsymbol{\sigma}_x$ Pauli matrix, and n is the number of qubits involved in the GHZ states). This state preparation is very similar to the generation of stabilizer operators [10], which are building blocks for quantum error correction codes. Furthermore, this algorithm takes the state of the quantum system to the most fragile reaches of the Hilbert space we are operating in and, therefore,

clearly demonstrates coherent control. Previous work has demonstrated a 12-spin pseudocat state [11] and multiple quantum coherences of much higher order [12]. However, these exploited symmetries in the systems which limited them to a much smaller symmetric subspace of the full Hilbert space. In the present Letter, we benchmark *universal* control methods that allow us to access the full Hilbert space of our system.

In a liquid state NMR QIP, universal control is achieved through the application of a coordinated sequence of radio-frequency (rf) pulses and periods of free evolution. The resulting 1- and 2-qubit gates allow us, in principle, to implement any unitary transformation [13]. The challenge is to efficiently design such pulse sequences to be as short as possible and robust against experimental imperfections in order to minimize systematic error and decoherence [14,15]. In a 3-qubit experiment [16], it is possible to write the pulse sequences by hand and compensate for experimental errors with a few optimization parameters. Moving to larger registers [1,8] requires more complex control schemes that necessitate systematic numerical optimization in the design of the pulse sequence. Going to 12 qubits represents a substantial step forward in the number of quantum degrees of freedom that are controlled.

We will approach coherent control over this large Hilbert space system from two complementary points of view. First, to demonstrate that control methods of high precision are available and experimentally realizable, we build a detailed model of the experimental QIP and, for each desired unitary operation, search for an optimal control sequence based on strongly modulating pulses [17]. Applied over the entire Hilbert space, this approach is not scalable. The amount of classical resources required to search for control sequences grows as the size of the Hilbert space—i.e., exponentially with the number of qubits. However, this approach returns control sequences of high fidelity and with small, known errors, provided our system model is accurate. Because of the exponential

computing cost of determining a suitable pulse, when deal-ing with a large Hilbert space, we have to lower the dimension of the space over which we search. This can be achieved by searching for pulses only on a subsystem of the spins of the register (in the present case, the carbon nuclear spins) and check that it leads to sufficiently high fidelity control by simulating the effect of rest of the spins as described in Ref. [18].

A second approach to control such a large Hilbert space is to make a series of well-constructed simplifications to the model, in order to permit control sequences to be developed with a complexity that grows only polynomially with the number of qubits. We therefore based the design of our pulse sequences on the method developed in Ref. [1]. Indeed, by using only simple pulses (broadband rectangular hard pulses and selective soft Gaussian shaped pulses) and performing a series of simulations on pairs of spins with significant couplings for each pulse, it is pos-sible to efficiently determine first-order deviations from the ideal pulse. For each of the pulses, these control errors can be represented as phase shifts and spin-spin coupling ef-fects occurring before and after an ideal pulse. One can then modify the phase of each pulse to correct for the phase shifts. Assuming that long range couplings between the spins vanish, the timing between pulses can be efficiently numerically optimized in order to absorb the coupling effects into the refocusing scheme [19]. This design does not take higher-order coupling and off-resonant effects into account and leaves some small couplings unrefocused to minimize the pulse sequence length. These approximations lead to errors in the control. A crucial point of this experi-mental work was to verify that these approximations hold for larger Hilbert spaces, i.e., that we could find a suitable refocusing scheme that, once optimized, still provides reliable control.

In liquid state NMR, the thermal equilibrium state is almost completely mixed. Therefore, instead of preparing ρ_{GHZ}, we actually prepare the following state:

$$\rho_{\text{cs}} \simeq \frac{\mathbf{I}^{\otimes N}}{2^N} + \epsilon \mathbf{X}^{\otimes n} \mathbf{I}^{\otimes (N-n)}, \tag{1}$$

$N = 14$ is the total number of spins-$1/2$ in the register, and n is the number of qubits involved in the GHZ state. The factor $\epsilon \simeq 10^{-5}$ is related to the thermal polarization of the system. The second term of ρ_{cs}, called the deviation den-sity matrix, contains the n-coherence term $|00\dots0\rangle \times \langle11\dots1| + |11\dots1\rangle\langle00\dots0|$ corresponding to a n-qubit cat state $|00\dots0\rangle + |11\dots1\rangle$, as well as lower coherence terms corresponding to the other n-qubit GHZ states. This state preparation (called the encoding of the pseudocat state) is done by propagating the polarization of the two equivalent protons through the chain of nuclei by a se-quence of 1- and 2-qubit quantum gates (see Fig. 1). In NMR, only single coherence terms are observable [20]. Therefore, to see the signature of the GHZ state, we need to transform the n-coherence term into a n-qubit labeled
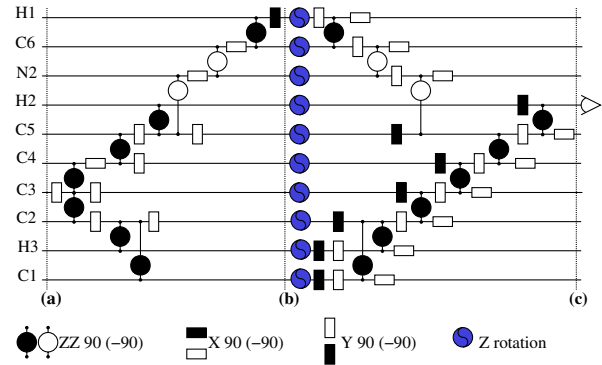

FIG. 1 (color online). Sequence of gates for the 10-qubit pseudocat-state preparation followed by its decoding into a 10-qubit pseudopure state. The initial preparation of the qutrit into a pseudopure state, as well as the refocusing gates, are not shown. Proper cycling of the Z rotations and the phase of observation act as a coherence filter. The qubit names corre-spond to the histidine molecule nuclei (see Fig. 2). (a) After the qutrit pseudopure preparation, the state of the register is $\mathbf{0}^{H_{4/5}}\mathbf{I}^{H_1}\mathbf{I}^{C_6}\mathbf{I}^{N_2}\mathbf{I}^{H_2}\mathbf{I}^{C_5}\mathbf{I}^{C_4}\mathbf{Z}^{C_3}\mathbf{I}^{C_2}\mathbf{I}^{H_3}\mathbf{I}^{C_1}$. At the end of the encod-ing in (b), it is $\mathbf{0XXXXXXXXXX}$, and, after filtering, the decoded state in (c) is $\mathbf{0000X000000}$.

pseudopure state of the form $\mathbf{X00\dots0}$ [where $\mathbf{0} = (\mathbf{I} + \mathbf{Z})/2$]. This step of the algorithm is called the decoding. To average away the other lower coherence order terms present in the $\mathbf{X}^{\otimes n}$ operator, we used two types of coher-ence filters: gradient and phase cycling techniques. Proof that we have actually created the pseudopure and accom-panying pseudocat state by determining the final state through tomography would require an impractically large number of experiments ($\sim 4^{12}$). Nevertheless, since the averaging procedure filters out the signal coming from every term but the desired one (i.e., the highest coherence order term), a single observation of the "read out" nucleus in the resulting NMR spectrum (see Fig. 2) indicates that we have indeed reached the desired coherence.

We applied both methods to design two series of pulse sequences that implement the encoding-decoding proce-dure, with n going from 1 to 12, on a liquid state NMR QIP, based on uniformly ^{13}C; ^{15}N labeled l-histidine (see Fig. 2). Two different samples were used. The one used for designing strongly modulating pulses was made of 16.7 mg of histidine and 15.9 mg of deuterated phosphoric acid in 1 ml of deuterated water. To design simplified pulse sequences, we prepared a second sample by dissolving 35.3 mg of histidine, 12.5 mg of glycine-2—^{13}C; ^{15}N, and 3.4 mg of deuterated phosphoric acid in 1 ml of deuterated water. The labeled glycine molecule has a sim-ple spectrum which allowed us to perform accurate cali-brations of the selective pulses on isolated NMR peaks *in situ*. The experiments based on the strongly modulating pulses and the simplified design were, respectively, per-formed on Avance-600 and Avance-700 Bruker spectrom-eters at Massachusetts Institute of Technology and Institute for Quantum Computing.
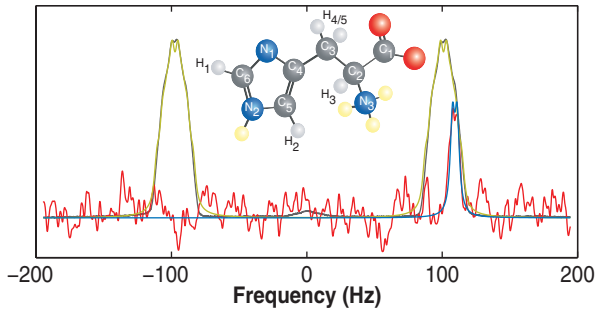
FIG. 2 (color).   This *l*-histidine molecule has 14 spin-1/2 nuclei: five ^{1}H, six ^{13}C, and three ^{15}N. See Ref. [24] for a more complete description of the molecule. The two protons H_4 and H_5, are chemically equivalent and indistinguishable. As such, they can be seen as a composite particle with a spin-1 and a spin-0 part. We considered only the spin-1 subspace (qutrit) since the spin-0 does not interact with the other spin-1/2. This molecule is therefore a 12-qubits plus one qutrit quantum register. However, the N_3 nuclear spin has a particularly weak coupling with the rest of the molecule; thus, we did not use it. On this plot, we have shown a reference spectrum of H_2 (gray plot) and of the pseudopure state obtained after decoding a 10-qubit cat state onto H_2 (red line). They are arbitrarily scaled for clarity. The reference spectrum was obtained with 2 scans and the pseudopure, with 4000 scans, in order to improve the signal to noise ratio. We also show simulated spectra of the expected reference (yellow plot) and pseudopure state (blue line) for which the amplitude is matched to the experimental data to evaluate the signal loss.

We based the design and the interpretation of the experiments on a model of the system and the apparatus [18] which includes the following attributes: (i) The Hamiltonian of the system in the static magnetic field of the spectrometer. The chemical shifts as well as the scalar-coupling strengths and relatives signs were experimentally determined by fits of reference spectra and small targeted multiple-coherence experiments. (ii) Knowledge of T_2 and T_2^* [20] relaxation times of the system. (iii) rf field inhomogeneities were mapped and used in the design of the strongly modulating pulses [21].

This type of experiment comes with a predicted exponential decay of signal as we increase the number of correlated qubits. We also expect high decoherence rates [22,23] and therefore a strong signal attenuation, as it is reasonable to assume that the relaxation rate for each spin included in the multiple quantum coherence add. To evaluate the quality of the control we could reach, the relevant quantity to measure is the amount of signal obtained experimentally with respect to the expected one assuming perfect control. Figure 3 shows how much signal we were able to retain after decoding the highest coherence order cat state into a pseudopure state for each experiment. We could reach a 12-coherence state using strongly modulating pulses and a 10-coherence state with selective pulses. Indeed, the sequences obtained through the simplified design were slightly longer, leading to more decoherence. Moreover, the transverse relaxation times were not the same in both sets of experiments. To distinguish between operational errors and relaxation loss, both decay times (T_2^* and T_2) were used to estimate the signal loss due to transversal relaxation during the pulse sequences (see Fig. 4). It showed that decoherence is the main source of signal loss and, therefore, indicates that we have good operational control.
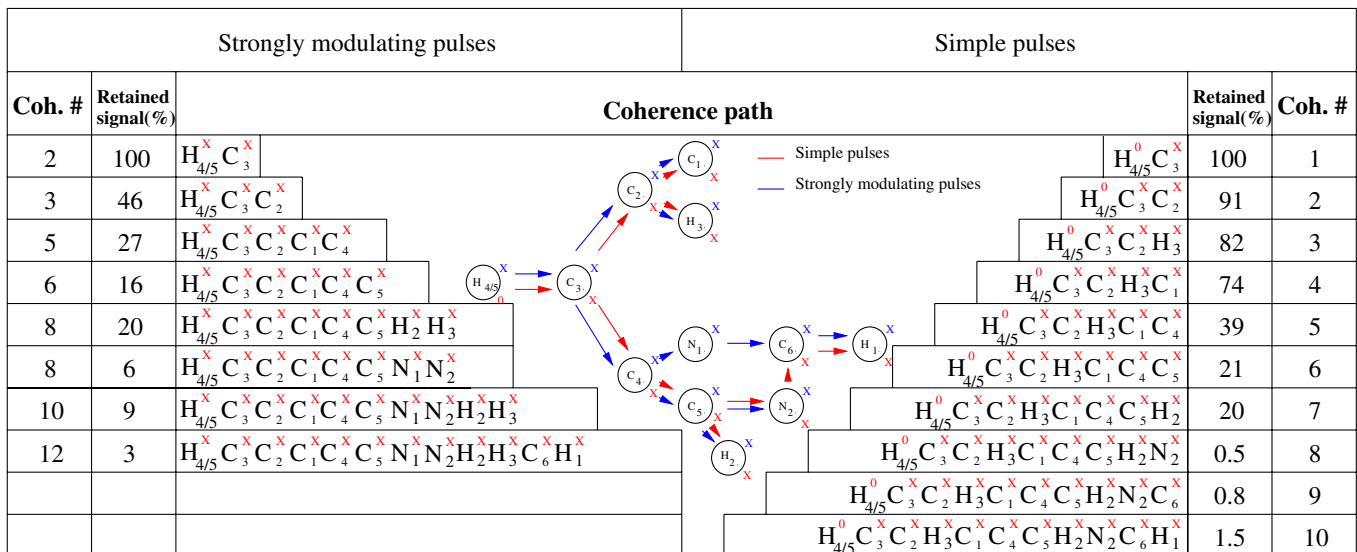
		Strongly modulating pulses	Simple pulses		
Coh. #	**Retained signal(%)**	**Coherence path**		**Retained signal(%)**	**Coh. #**
2	100	$H^X_{4/5} C^X_3$	$H^0_{4/5} C^X_3$	100	1
3	46	$H^X_{4/5} C^X_3 C^X_2$	$H^0_{4/5} C^X_3 C^X_2$	91	2
5	27	$H^X_{4/5} C^X_3 C^X_2 C^X_1 C^X_4$	$H^0_{4/5} C^X_3 C^X_2 H^X_3$	82	3
6	16	$H^X_{4/5} C^X_3 C^X_2 C^X_1 C^X_4 C^X_5$	$H^0_{4/5} C^X_3 C^X_2 H^X_3 C^X_1$	74	4
8	20	$H^X_{4/5} C^X_3 C^X_2 C^X_1 C^X_4 C^X_5 H^X_2 H^X_3$	$H^0_{4/5} C^X_3 C^X_2 H^X_3 C^X_1 C^X_4$	39	5
8	6	$H^X_{4/5} C^X_3 C^X_2 C^X_1 C^X_4 C^X_5 N^X_1 N^X_2$	$H^0_{4/5} C^X_3 C^X_2 H^X_3 C^X_1 C^X_4 C^X_5$	21	6
10	9	$H^X_{4/5} C^X_3 C^X_2 C^X_1 C^X_4 C^X_5 N^X_1 N^X_2 H^X_2 H^X_3$	$H^0_{4/5} C^X_3 C^X_2 H^X_3 C^X_1 C^X_4 C^X_5 H^X_2$	20	7
12	3	$H^X_{4/5} C^X_3 C^X_2 C^X_1 C^X_4 C^X_5 N^X_1 N^X_2 H^X_2 H^X_3 C^X_6 H^X_1$	$H^0_{4/5} C^X_3 C^X_2 H^X_3 C^X_1 C^X_4 C^X_5 H^X_2 N^X_2$	0.5	8
			$H^0_{4/5} C^X_3 C^X_2 H^X_3 C^X_1 C^X_4 C^X_5 H^X_2 N^X_2 C^X_6$	0.8	9
			$H^0_{4/5} C^X_3 C^X_2 H^X_3 C^X_1 C^X_4 C^X_5 H^X_2 N^X_2 C^X_6 H^X_1$	1.5	10

(Coherence path diagram legend: — Simple pulses; — Strongly modulating pulses)

FIG. 3 (color online).   Description of each of the multiple-coherence experiments. The picture shows how the polarization of the $H_{4/5}$ is propagated through the nuclei chain to create the cat state. In the series of experiments using simple pulses, we first prepared the qutrit made of the two equivalent protons into a pseudopure state $\mathbf{0} = (\mathbf{I} + \mathbf{Z})/2$ and left it as such for the rest of the experiments. When using strongly modulating pulses, we included the qutrit into the multiple-coherence state. The two first and two last columns show the coherence number we reached and how much signal we were able to retain after decoding the cat state into a observable pseudopure state. Results are shown in percentage of the expected signal assuming perfect control, normalized to the first experiment.

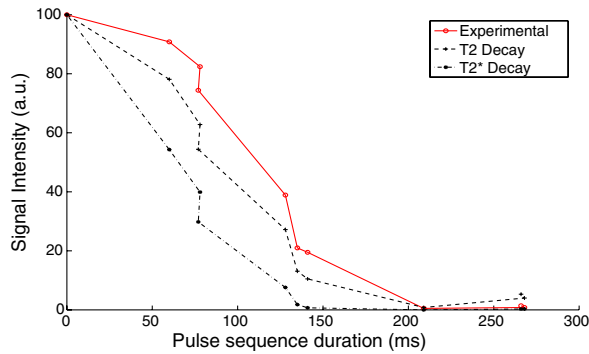P H Y S I C A L   R E V I E W   L E T T E R S

FIG. 4 (color online).   Expected decay of the pseudopure state signal due to transversal relaxation for the series of experiments done with simple pulses. Each point corresponds to a different coherence experiment. The length of the pulse sequence increases with the coherence order. Most experimental points are above the estimates given by T_2^* and even T_2. Indeed, to predict the transversal relaxation during the pulse sequence, we used only a very simple model of decay for multiple coherences that gives an upper bound of the signal loss. Nevertheless, the experimental curve and predicted ones show the same decay pattern. Thus, it is reasonable to say that most of the signal loss comes from decoherence and, therefore, that we have a good operational control over the system. For the coherences 8, 9, and 10 (last three points), the experimental curve goes below the T_2 curve. It reflects a loss of accuracy in our operational control. Indeed, for these experiments, we are controlling the nitrogen nuclei through very small couplings. We are, therefore, using long 2-qubits gates that are sensitive to any small inaccuracy in the values of the Hamiltonian parameters.

In summary, we have reported an algorithmic benchmark performed on the largest quantum information processor to date. Despite the decoherence during the computation, we have been able to demonstrate universal control on up to 11 qubits and one qutrit. This work shows that liquid state NMR allows us to develop operational control methods that can be used to control a large number of quantum degrees of freedom. These methods provide a systematic and efficient way of programming liquid state NMR QIPs. However, the approaches and control techniques behind these methods could also be used to design control sequences in more scalable implementations where the intrinsic errors are smaller.

[1] E. Knill, R. Laflamme, R. Martinez, and C.-H. Tseng, Nature (London) **404**, 368 (2000).

[2] A. Furusawa, J. Sorensen, S. L. Braunstein, C. Fuchs, H. J. Kimble, and E. S. Polzik, Science **282**, 706 (1998).
[3] M. Riebe *et al.*, Nature (London) **429**, 734 (2004).
[4] M. D. Barret *et al.*, Nature (London) **429**, 737 (2004).
[5] D. P. DiVincenzo and P. W. Shor, Phys. Rev. Lett. **77**, 3260 (1996).
[6] N. Gershenfeld and I. L. Chuang, Science **275**, 350 (1997).
[7] D. G. Cory, A. F. Fahmy, and T. F. Havel, Proc. Natl. Acad. Sci. U.S.A. **94**, 1634 (1997).
[8] L. M. K. Vandersypen, M. Steffen, G. Breyta, C. S. Yannoni, M. H. Sherwood, and I. L. Chuang, Nature (London) **414**, 883 (2001).
[9] E. Knill, R. Laflamme, R. Martinez, and C. Negrevergne, Phys. Rev. Lett. **86**, 5811 (2001).
[10] D. Gottesman, Ph.D. thesis, California Institute of Technology, Pasadena, CA, 1997, quant-ph/9705052.
[11] J.-S. Lee and A. K. Khitrin, J. Chem. Phys. **122**, 041101 (2005).
[12] W. S. Warren, D. P. Weitekamp, and A. Pines, J. Chem. Phys. **73**, 2084 (1980).
[13] A. Barenco, C. H. Bennett, R. Cleve, D. P. DiVincenzo, N. Margolus, P. Shor, T. Sleator, J. Smolin, and H. Weinfurter, Phys. Rev. A **52**, 3457 (1995).
[14] N. Khaneja, R. Brockett, and S. J. Glaser, Phys. Rev. A **63**, 032308 (2001).
[15] J. A. Jones, Phys. Rev. A **67**, 012317 (2003).
[16] D. Cory, M. D. Price, W. Maas, E. Knill, R. Laflamme, W. Zurek, T. F. Havel, and S. S. Somaroo, Phys. Rev. Lett. **81**, 2152 (1998).
[17] E. M. Fortunato, M. A. Pravia, N. Boulant, G. Teklemariam, T. F. Havel, and D. G. Cory, J. Chem. Phys. **116**, 7599 (2002).
[18] Y. S. Weinstein, T. F. Havel, J. Emerson, N. Boulant, M. Saraceno, S. Lloyd, and D. G. Cory, J. Chem. Phys. **121**, 6117 (2004).
[19] M. D. Bowdrey, J. Jones, R. Laflamme, and M. Knill, Phys. Rev. A **72**, 032315 (2005).
[20] R. R. Ernst, G. Bodenhausen, and A. Wokaun, *Principles of Nuclear Magnetic Resonance in One and Two Dimensions* (Oxford University Press, Oxford, 1994).
[21] M. Pravia, N. Boulant, J. Emerson, A. Farid, E. Fortunato, T. Havel, R. Martinez, and D. Cory, J. Chem. Phys. **119**, 9993 (2003).
[22] H. Krojanski and D. Suter, Phys. Rev. Lett. **93**, 090501 (2004).
[23] J.-S. Lee and A. K. Khitrin, quant-ph/0508052.
[24] See EPAPS Document No. E-PRLTAO-96-009617 for a figure that describes in more detail the histidine molecule used in the experiments. The table includes chemical shifts, *J*-coupling values, and relaxation times (*T*2 and *T*2*). For more information on EPAPS, see http://www.aip.org/pubservs/epaps.html.